14th International Conference on Information Fusion
Chicago, Illinois, USA, July 5-8, 2011

Dismount Tracking by Fusing Measurements from a Constellation of Bistatic Narrowband Radar

Chris Kreucher
Sensors and Analysis Group
Integrity Applications Incorporated
900 Victors Way, Suite 220, Ann Arbor MI 48108
ckreucher@integrity-apps.com

Abstract*[1] — *This paper presents a nonlinear filtering approach to detecting and tracking moving targets from a constellation of narrowband radio frequency sensors. The methodology optimally fuses bistatic range and range-rate measurements made by a collection of sensors without thresholding or linear/Gaussian assumptions. We illustrate the efficacy of the algorithm with an experiment where a moving person is detected and tracked from a constellation of 4 sensors using measurements of bistatic range and range-rate. We use a narrowband radar because of its practical benefits and illustrate successful tracking of a moving dismount with just 5 meters of range resolution.

Keywords: Dismount tracking, bistatic range, bistatic Doppler, multisensor fusion, nonlinear filtering

1 Introduction

This paper describes a method of detecting and tracking moving targets by exploiting a constellation of bistatic narrowband (NB) Radio Frequency (RF) sensors positioned in and around a surveillance region. We give a Bayes-optimal method for fusing the received bistatic range/range-rate measurements from the constellation of sensors to effectively locate the moving target. We illustrate the efficacy of the method experimentally by showing how a moving person is tracked in a surveillance region interrogated by four NB sensors.

A constellation of narrowband sensors has a number of benefits over conventional wideband sensors in this application. First, commercial use has eroded the available spectrum often leaving only a small portion available for other use [1]. Furthermore, NB sensors are inexpensive due to their simple electronics, require low energy consumption, are easy to maintain, and it is easy to communicate their data to a centralized processing point. But perhaps most importantly, a constellation of NB sensors provide geometric diversity. By exploiting bistatic returns with advanced signal processing techniques like those described here, this trades costly spectral diversity for cost-efficient spatial diversity, while providing performance improvement.

The contributions of this paper are the description of a Bayes optimal nonlinear filtering method which admits the nonlinear and non-Gaussian measurements made by the sensors, and a validation of its assumptions using real, collected data from a 4 antenna bistatic radar setup.

Standard approaches use two sequential phases: detection and tracking. One algorithm is responsible for generating threshold exceedances (detections) at each time epoch and then these detections are passed to a separate (typically Kalman-based) tracking algorithm.

In contrast, the nonlinear filtering approach performs track-before-detect and fuse-before-track. A number of other authors have done important related work [2]-[7]. The important distinction of the techniques is that there measurement thresholding is avoided. Furthermore, the non-Gaussian measurement statistics and non-linear measurements are modeled directly rather than by linearization.

Target tracking using multistatic range and range-rate measurements has received some attention in the literature. [8]-[10] approach the problem using a direct measurement model with Gaussian error, rather than the pixelated Rayleigh model we use here. [9][10] use extended Kalman filter type approaches, rather than the nonlinear filtering approach we use. [11] treats the problem with a nonlinear filtering approach, but in a active sonar setting, which requires a very different physical model.

The paper proceeds as follows. Section 2, describes the bistatic range and range-rate signal model. In Section 3, we show how the model is combined with a nonlinear filter to provide a tractable Bayes optimal tracking approach. In Section 4, we describe a set of experiments where we collected narrowband bistatic range and range-rate data from a four-antenna constellation, and the measurements were used to validate the tracking algorithm and modeling approach. Finally, section 5 concludes.

[1] This work was supported by Air Force Research Labs contracts FA8650-09-M-1549 and FA8650-10-C-1718.

2 The Sensor Model

We assume a constellation of N sensors, all of which act as both transmitters and receivers, although this is not required. A sensor transmits a narrowband RF signal, which is reflected off the target and received at each sensor. This process repeats *N-1* times, with each sensor serving as transmitter. There are then N^2 bistatic pairs.

After a CPI of pulses has been transmitted, Fourier processing is used to translate the received samples into a (bistatic) range/range-rate surface for each transmit/receive pair. This surface contains energy at the target bistatic range/range-rate bin (and perhaps surrounding bins) and is corrupted by various types of noise, including clutter, measurement noise, and quantization noise.

We employ the following statistical model to describe the measurements. First, let $z_{ij}(t,r)$ denote the magnitude in the $(i,j)^{th}$ bistatic range/range-rate resolution cell between transmitter t and receiver r. Resolution and the number of cells (denoted N_r and N_d here) are determined by the number of pulses, bandwidth, CPI and PRF [17]. The collection of measurements is then the matrix of bistatic range/range-rate correlations in each cell, i.e.,

$$z(t,r) = \begin{pmatrix} z_{11}(t,r) & \cdots & z_{1Nd}(t,r) \\ & \cdots & \\ z_{Nr1}(t,r) & \cdots & z_{NrNd}(t,r) \end{pmatrix} \tag{1}$$

Next, let the vector $x = [\mathrm{x}\ \mathrm{x}'\ \mathrm{y}\ \mathrm{y}']$ describe the true 2D position and velocity of the target. The statistics of the measurement in bistatic range/range-rate cell *(i,j)* depend on its proximity to the true bistatic range and range-rate of the target. Other factors such as the range to the target, the illumination and receive pattern of the antenna may also play a role, but are not important in our experiments, which use a close-in target with large beamwidth antennas, so these effects are not modeled here.

The location of the transmitter t will be denoted (t_x, t_y), and the location of receiver r will be denoted (r_x, r_y). Then the true bistatic range and range-rate is computed as

$$R(x,t,r) = \sqrt{(\mathrm{x}-\mathrm{r_x})^2 + (\mathrm{y}-\mathrm{r_y})^2} + \sqrt{(\mathrm{x}-\mathrm{t_x})^2 + (\mathrm{y}-\mathrm{t_y})^2} \tag{2}$$

and

$$\dot{R}(x,t,r) = \frac{\mathrm{x}'(\mathrm{x}-\mathrm{r_x}) + \mathrm{y}'(\mathrm{y}-\mathrm{r_y})}{\sqrt{(\mathrm{x}-\mathrm{r_x})^2 + (\mathrm{y}-\mathrm{r_y})^2}} + \frac{\mathrm{x}'(\mathrm{x}-\mathrm{t_x}) + \mathrm{y}'(\mathrm{y}-\mathrm{t_y})}{\sqrt{(\mathrm{x}-\mathrm{t_x})^2 + (\mathrm{y}-\mathrm{t_y})^2}} \tag{3}$$

This true bistatic range/range-rate maps to a particular cell, which we will denote *(î(t,r), ĵ(t,r))*. We use a point-target model, which ignores extended target effects such as sidelobes, the range-rate smearing which will happen in applications with a long CPI, and range extent which will happen with fine range resolution (high bandwidth). Since our application uses a short CPI and a small bandwidth, the point target assumption is warranted. The extension to non-point target models is straightforward but is not necessary in this application.

The physical model we employ says the statistics of the target cell are Rayleigh with a target parameter and the statistics of the background cells are Rayleigh with a background parameter:

$$p\left(z_{ij}(t,r) \mid x\right) = \begin{cases} 2\frac{z_{ij}(t,r)}{\lambda_t^2}\exp\left(-\frac{z_{ij}^2(t,r)}{\lambda_t^2}\right) & i,\ j = \hat{i}(t,r),\ \hat{j}(t,r) \\ 2\frac{z_{ij}(t,r)}{\lambda_b^2}\exp\left(-\frac{z_{ij}^2(t,r)}{\lambda_b^2}\right) & i,\ j \neq \hat{i}(t,r),\ \hat{j}(t,r) \end{cases} \tag{4}$$

Where λ_β and λ_τ are the target and background modes. This model is verified empirically in Section 4.

In general, we allow the background and target mode parameters to vary with t and r, but for the sake of notational clarity we show them fixed here. Continuing with the point target model, which assumes measurements in different pixels are independent, we write

$$\begin{aligned} p\left(z(t,r) \mid x\right) &= \prod_{i=1}^{Nr}\prod_{j=1}^{Nd} p\left(z_{ij}(t,r) \mid x\right) \\ &= p\left(z_{\hat{i}(t,r),\hat{j}(t,r)}(t,r) \mid x\right) \prod_{\substack{i=1 \\ i,j\neq\hat{i}(t,r),\hat{j}(t,r)}}^{Nr}\prod_{j=1}^{Nd} p\left(z_{ij}(t,r) \mid x\right) \\ &\propto \frac{\lambda_b}{\lambda_t}\exp\left(\frac{z^2_{\hat{i}(t,r),\hat{j}(t,r)}(t,r)(\lambda_t^2-\lambda_b^2)}{\lambda_b^2\lambda_t^2}\right) \end{aligned} \tag{5}$$

as the probability of a N_r x N_d range/range-rate surface given the true state x. We further assume range/range-rate surfaces are statistically independent across transmit/receive pairs and write the probability of all of the bistatic range/range-rate measurements from a constellation of transmit/receive antennas as

$$\begin{aligned} p\left(z \mid x\right) &= \prod_t\prod_r p\left(z(t,r) \mid x\right) \\ &\propto \prod_t\prod_r \frac{\lambda_b}{\lambda_t}\exp\left(\frac{z^2_{\hat{i}(t,r),\hat{j}(t,r)}(t,r)(\lambda_t^2-\lambda_b^2)}{\lambda_b^2\lambda_t^2}\right) \end{aligned} \tag{6}$$

3 Bayesian Detection and Tracking

This section describes a Bayes-optimal single target tracking algorithm that fuses measurements from a constellation of narrowband radar.

3.1 Notation

Denote the state of a target at time k as x^k, which for this work refers to the targets' 2D position and velocity, i.e., $x^k = [\text{x x}' \text{ y y}']$. Additionally, let H^k_0 denote the hypothesis that no target is present at time k, and let H^k_1 denote the hypothesis that a target is present.

Measurements continue to be described as follows:

- The envelope-detected value in range/range-rate cell *(i,j)* at CPI k from transmitter t and receiver r is denoted $z_{ij}^k(t,r)$,
- The collection of all $z_{ij}(t,r)$ made at a particular CPI is denoted $z^k(t,r)$, i.e., $z^k(t,r)=\{z_{11}^k(t,r),\ldots, z_{NrNd}^k(t,r)\}$;
- The collection of all measurements made at a particular CPI k (i.e., from all transmit receive pairs) is denoted simply z^k, i.e., $z^k = \{z^k(1,1), \ldots, z^k(T,R)\}$.
- Finally, Z^k will denote the collection of all measurements received up to and including time k, i.e., $Z^k = \{z^1,\ldots, z^k\}$.

3.2 Approach

The Bayesian method is to estimate the joint probability a target is present (H^k_1 is true) at each state x^k given the measurements. Mathematically, this means we wish to estimate the hybrid continuous-discrete probability density function (PDF)

$$p(x^k, H_1^k \mid Z^k) \tag{7}$$

for all x^k, as well as the discrete probability

$$p(H_0^k \mid Z^k) = 1 - \int p(x^k, H_1^k \mid Z^k) dx^k \tag{8}$$

Notice we can write

$$p(x^k, H_1^k \mid Z^k) = p(H_1^k \mid Z^k)\, p(x^k \mid H_1^k, Z^k) \tag{9}$$

i.e., the density is the product of the *target present probability* $p(H_1^k|Z^k)$ and the *target state probability* $p(x^k|H_1^k,Z^k)$. Both conceptually and in implementation, we treat the problem as separate (but coupled) tasks of estimating the target present probability and the estimating target state probability.

In the Bayesian approach, we (i) assume an initial or prior estimate of the desired probabilities is present (perhaps completely uninformative), and (ii) generate a recursive formula that relates probabilities at one time step with those at the next. This is done in two steps, analogous to the Kalman Filter: the temporal update, which predicts the probability distribution at time k from that at time k-1, and the measurement update which corrects the predicted probability distribution at time k given the measurements received at time k.

The first step in recursive Bayesian filtering is to predict the relevant probability distributions forward in time using statistical models on target kinematics. The temporal update of the target present density is

$$p(H_1^k \mid Z^{k-1}) = \sum_{i=0}^{1} p(H_1^k \mid Z^{k-1}, H_i^{k-1}) p(H_1^k \mid Z^{k-1}) \tag{10}$$

where the quantity $p(H_1^k|Z^{k-1},H_i^{k-1})$ is a statistical model to be specified by studying the target arrival properties.

Similarly, the time-predicted target state density is based on a model of how targets move

$$p(x^k \mid H_1^k, Z^{k-1}) = \left(\frac{p\left(H_1^{k-1} \mid Z^{k-1}\right)}{p\left(H_1^k \mid Z^{k-1}\right)} \right) * \int p(x^k, H_1^k \mid x^{k-1}, H_1^{k-1})\, p(x^{k-1} \mid H_1^{k-1}, Z^{k-1}) dx^{k-1} \tag{11}$$

where the density $p(x^k,H_1^k|\ x^{k-1},H_1^{k-1})$ is a statistical model on target kinematics to be specified in the particular implementation. The normalizing term does not need to be
evaluated as the density can be forced to integrate to 1. In this work, we assume the nearly constant velocity (NCV) model for the target. Other models, or even multiple models are admissible under the Bayesian framework [12].

3.3 Measurement Update

The second step in Bayesian filtering is to accommodate measured data into the probability estimate. The measured data comes into the picture through the sensor model $p(z^k|H_1^k,x^k)$, where the functional form of is the model specified by sensor physics from Section 2.

The target present and target absent probabilities are measurement updated using the law of total probability and Bayes rule, yielding

$$\begin{aligned} p(H_1^k \mid Z^k) &= \left(\frac{p(H_1^k \mid Z^{k-1})}{p(z^k \mid Z^{k-1})} \right) x \\ &\quad \int p(z^k \mid H_1^k, x^k)\, p(x^k \mid H_1^k, Z_1^k) dx^k \\ p(H_0^k \mid Z^k) &= \left(\frac{p(H_0^k \mid Z^{k-1})}{p(z^k \mid Z^{k-1})} \right) p(z^k \mid H_0^k) \end{aligned} \tag{12}$$

This equation expresses the current target present and absent hypothesis probabilities in terms of the target

present, target absent, and target state probabilities predicted from the previous time step and the conditional likelihood of incoming measurements. The normalization constant does not need to be computed since $p(H_1^k|Z^k)+p(H_0^k|Z^k)=1$.

The target state probability is updated similarly,

$$p(x^k \mid H_1^k, Z^k) = p(x^k \mid H_1^k, Z^{k-1}) \left(\frac{p(z^k \mid x^k, H_1^k)}{p(z^k \mid H_1^k, Z^{k-1})} \right) \quad (13)$$

Again, constants independent of x^k do not need to be computed.

In our application which exploits bistatic pixilated range/range-rate measurements, the model developed in Section 2, eq. (6) provides $p(z^k|H_1^k,x^k)$.

3.4 Implementation

If the probability density of interest is well approximated by a Gaussian or sum-of-Gaussians, techniques such as the Extended Kalman Filter or Gaussian Sum Filter are preferred. In the bistatic RF case we study here where we make measurements of bistatic range and range-rate, however, the density is poorly approximated by such parameterizations. We instead rely on a discrete grid approximation to the probability density.

The details of the discrete grid implementation are briefly reviewed here. For more detail, see [12][13][14].

1) Density Representation: The PDF of x is discretized onto a 4D grid (corresponding to the four dimensional state vector x^k) of *Nx*Nx'*Ny*Ny*' cells. The spatial extent of this grid dictates the overall region where targets may be detected. This approximation is appropriate here, given we wish to perform surveillance over a region of fixed spatial extent.

2) Kinematic and Measurement Updates: The temporal evolution of the probability density on x^k can be expressed in continuous time using a partial differential equation. For dismount tracking, the so-called nearly constant velocity model (NCV) is appropriate, and leads to the Fokker-Plank Equation [15][16]

$$\frac{\partial p}{\partial t} = -\dot{x}\frac{\partial p}{\partial x} - \dot{y}\frac{\partial p}{\partial y} + \frac{\sigma_{\dot{x}}^2}{2}\frac{\partial^2 p}{\partial \dot{x}^2} + \frac{\sigma_{\dot{y}}^2}{2}\frac{\partial^2 p}{\partial \dot{y}^2} \quad (14)$$

Computationally, the state probability is discretized onto the grid and the update is computed from time k-1 to k using a backward Euler method. This approach has nice stability properties in both δt and δx. We use Thomas' algorithm as a fast tridiagonal solver leading to computation linear in the number of grid cells. For more details, see [12][13]. The temporal evolution of the target present probability assumes constant target arrival/removal.

New measurements are incorporated by updating the time-predicted grid approximation using the likelihood of the measurements. Practically, the discrete grid probability is updated simply by pointwise multiplication of each cell in the discrete representation by the corresponding data likelihood.

4 Experimental Results

This section describes an experiment to validate the nonlinear filtering algorithm described in Section 3. The experiment consists of a set of four geometrically diverse antennas which measure information about bistatic range and range-rate of a moving dismount. We show with this experimental data that our algorithm is able to detect and track the dismount as it moves though the surveillance region using just *60MHz* of bandwidth (*5m* bistatic range resolution).

4.1 Test Hardware

The experiment we describe here employed an AKELA AVMU500A radar along with 4 *SAS-510-4* antennas. The antennas are directional and are specified to have a *3dB* point of *41* degrees by the manufacturer. The system was selected because its size and versatility demonstrate the ability of a compact, contained system to effectively collect the necessary data.

The radar is a stepped CW type, capable of transmitting pulses between *300MHz* and *3GHz*. The rate at which the individual frequencies are sampled is selectable, but typically set here at *45kHz* which is the maximum rate where good data was collected. The radar has four ports, any of which may be used for transmit or receive, however, because the radar has only one transmitter and receiver, it is not possible to receive multiple ports simultaneously. Therefore the collections will transmit and receive between one pair, and then move to transmit and receive to the next pair, and so on. Since this happens at a very fast rate compared to the dismount speed, the measurements are well approximated as being simultaneous.

Figure 1 shows one of the antennas as-deployed and the AKELA unit.

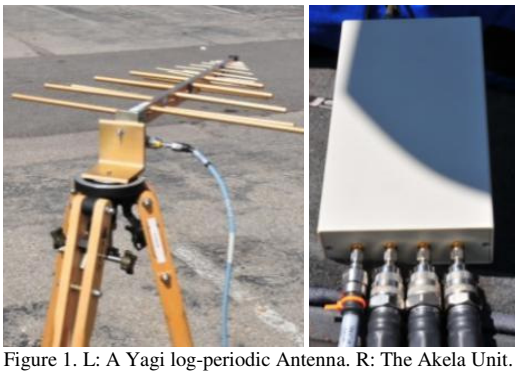

Figure 1. L: A Yagi log-periodic Antenna. R: The Akela Unit.

4.2 Experiment Setup

Four antennas were arranged along a *35m* line as illustrated in the image of Figure 2. GPS measurements of the antenna locations were measured with a hand-held unit, but there may have been an error as much as *½m* in placing the GPS units.

Figure 2. The Four antenna configuration used in this experiment.

Figure 3 is an image of the surveillance region with the relevant experimental information superimposed. The four antennas were located at *y=0* and *x=0, 10, 20,* and *35m* as indicated by the red circles and associated numbers. The antennas were pointed at the scene center (indicated by a green circle). The path walked by the dismount during this experiment is indicated by a dashed green line.

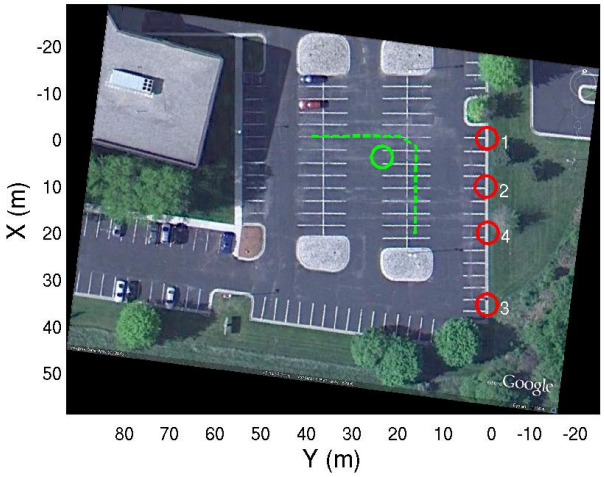

Figure 3. A view of the surveillance region with the four antennas denoted by red circles. All antennas point at scene center (denoted by the green circle). This dismount walks the dashed green path.

We collected bistatic measurements using antenna *3* as the transmitter and the other antennas (*1, 2*, and *4*) as receivers. We chose to use *60MHz* of bandwidth centered around *2GHz* with *20* sample frequencies (i.e., pulses spaced *3MHz* in frequency) in the collect. These choices determine the range resolution, the unambiguous range, and indirectly the range-rate resolution.

In this stepped chirp single-radar multiple antenna system, the collections proceeded as follows: First, antenna *3* transmitted a short pulse at the lowest frequency (*1.97GHz*) which was received by antenna *1*. Then antenna *3* transmitted a short pulse at the second lowest frequency (*1.973GHz*), which was received by antenna *1*, and so on until the highest frequency (*2.03GHz*).was completed. Once the final pulse between antenna *3* and antenna *1* was completed, the process was repeated between antenna *3* and antenna *2*, and then between antenna *3* and antenna *4*. The individual sweep pulses proceeded at *45kHz*, but the overall rate is dictated by the number of sweep pulses per pair (here *20*), the number of bistatic pairs (here there are 3 pairs), and the switching times. In this experiment, the actual complete cycle PRF (measured between the time the first sweep pulse is transmitted between antenna 3 and antenna 1 and then repeated again) was 150Hz.

4.3 Collected Data

RF data was collected while a dismount moved through the surveillance region over about a *40*s period. The path was truthed with a handheld GPS unit. Figure 4 shows an image of the dismount walking during the experiment.

Figure 4. An image of the dismount walking.

Data was collected between the transmitter (antenna *3*) and the three receivers (antennas *1, 2*, and *4*). The received complex frequency returns were blocked up into a *0.25s* CPI, and Fourier transformed into a range/range-rate matrix as described in Section 2. The resulting input data surface had *20* range bins spanning example of the input data surface is shown in Figure 5.

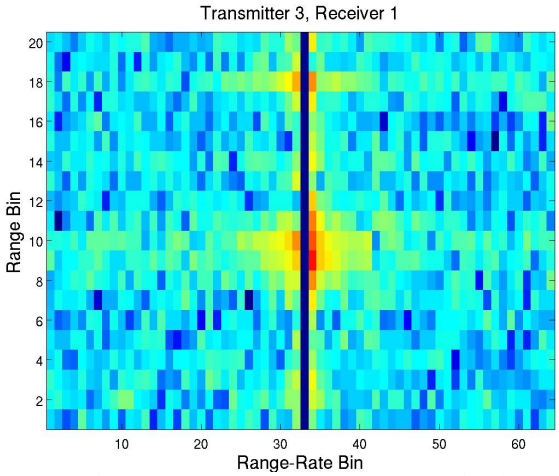

Figure 5. An example collected range/range-rate surface from Transmitter 3 to Receiver 1. The dismount is visible at range bin 10, and a second, transient, mover is visible at range bin 18.

Figure 5 shows the collected data when it is only compressed in the range direction (i.e., it is not blocked up into CPI and compressed in the range-rate direction).

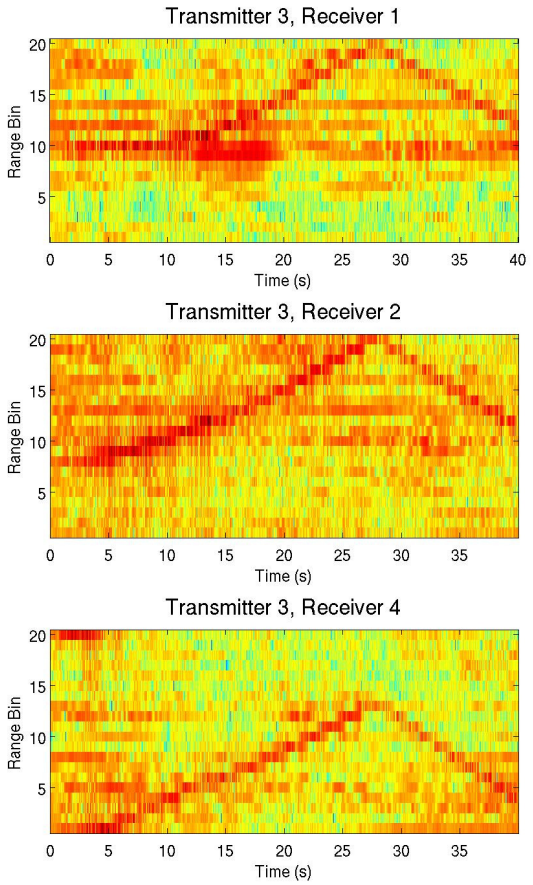

Figure 6. The *40s* of collected data from each of the bistatic pairs. Visible is direct path energy, electronic noise, and the effect of ambiguous range.

Figure 7 (right) shows the statistics in the background pixels (non-target containing pixels) and in the target pixel are both Rayleigh. This experimentally verifies the assumption we made in Section 2.

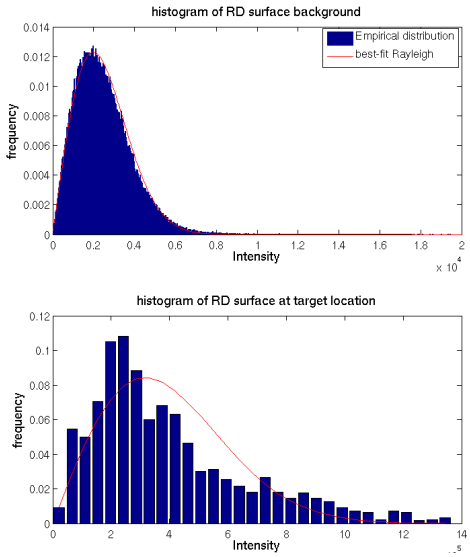

Figure 7. Background and target statistics of a measured surface.

We employed the nonlinear filter based target tracker described in Section 3 above. We used a *31x21x31x21* grid and a *60m x 16m/s x 60m x 16m/s* region. Tracking results using *5m* of range resolution are very successful as illustrated in Figure 8, which compares the tracker estimate of dismount position with GPS recordings of the path location. Notice the very close agreement between the tracker point estimate and the GPS value of path location. Although the tracker computes a complete *4D* PDF on target state, the uncertainly can be summarized using covariance ellipses. In this figure, we have chosen to show covariance ellipses at the start, middle, and end of the vignette. Note that the GPS measurements were not differentially corrected so there is some error the estimate of path truth and of the transmitter/receiver locations.

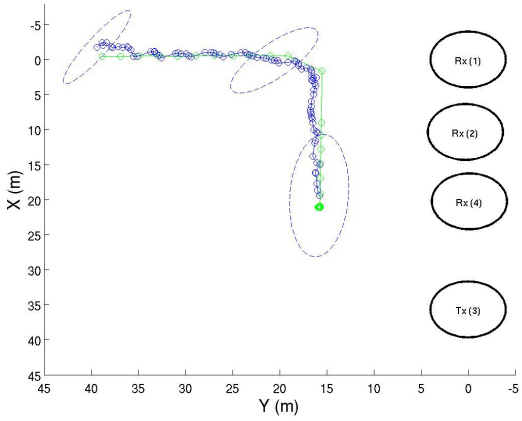

Figure 8. Tracking results using 3 bistatic pairs and 5m range resolution. Tracker covariance ellipses at the start, middle, and end of the path are shown. GPS truth is shown in green.

An illustration of the richness with which the tracker estimates the target state is given in Figure 9, where we show the XY marginal of the posterior.

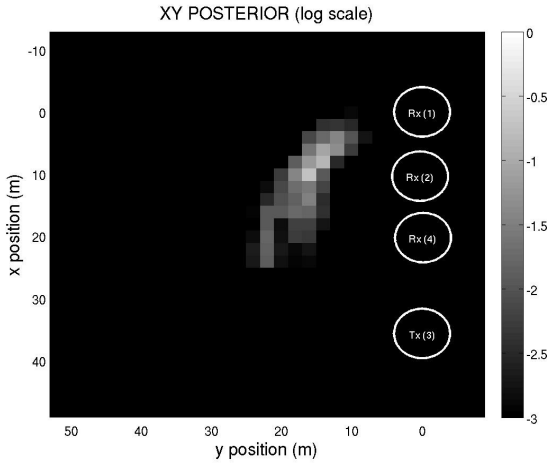

Figure 9. The XY marginal of the posterior shows the tracker uncertainty about target location at a particular instant.

The probability of target existence, $p(H_1^k \mid Z^k)$ grows quickly to 1 and stays as illustrated in Figure 10.

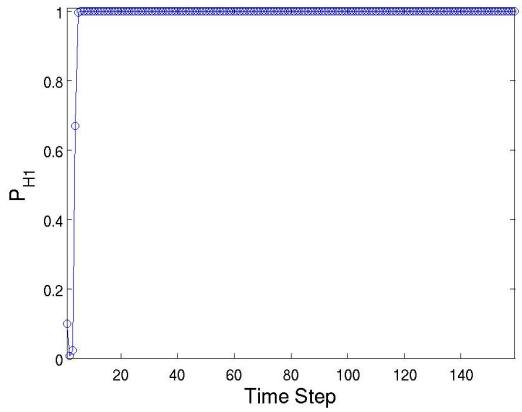

Figure 10. The tracker probability that there is a target in the surveillance region very quickly goes to 1 and stays there.

5 Conclusion

This paper has presented a nonlinear filtering approach to detecting and tracking moving targets using a constellation of narrowband radio frequency (RF) sensors. We use a narrowband radar because of a number of practical benefits discussed in the paper.

The nonlinear filtering methodology optimally fuses bistatic range and range-rate measurements made by a collection of sensors without thresholding or linear/Gaussian assumptions, thereby improving the detection/false alarm tradeoff and lowering tracking error.

We have illustrated the efficacy of the algorithm using real data experiments, where a moving person is detected and tracked from a constellation of 4 sensors using measurements of bistatic range and range-rate. The method shows successful tracking of a moving dismount with just 5 meters of range resolution.

6 Acknowledgements

The author would like to gratefully acknowledge the assistance of Ben Hart, Chris Roussi, Joe Burns, and Mike Brennan who assisted with the collection of the experimental data used to validate this approach.

7 References

[1] B. Himed, H. Bascom, J. Clancy and M. Wicks, *Tomography of moving targets*, Proceedings of SPIE, the International Society for Optical Engineering, 2001, vol. 4540, pp. 608-619.

[2] Y. Boers, J. N. Driessen, *Multi-target particle filter track before detect application*, IEE Proc. RSN, Vol.151, No.6, Dec. 2004.

[3] M Rutten, N. Gordon, and S. Maskell, *Particle-based track-before-detect in Rayleigh noise*, Proc. SPIE vol. 5428, pp. 509-519, August 2004.

[4] R. Bethel and G. Paras, *A PDF multisensor Multitarget Tracker*, IEEE Transactions on AES, vol. 34, no. 1, pp. 153–168, January 1998.

[5] L. Stone, C. Barlow, and T. Corwin, *Bayesian Multiple Target Tracking*. Boston: Artech House, 1999.

[6] K. Kastella, *Joint Multitarget Probabilities for Detection and Tracking*, in Proceedings of SPIE Acquisition, Tracking and Pointing XI, 1997.

[7] M. S. Arulampalam, S. Maskell, N. Gordon, and T. Clapp, *A Tutorial on Particle Filters for Online Nonlinear/non-Gaussian Bayesian Tracking*, IEEE Trans. on SP, vol. 50, no. 2, pp. 174–188, Feb. 2002.

[8] M. Tobias and A. Lanterman, *Probability hypothesis density-based multitarget tracking with bistatic range and Doppler observations*, Radar, Sonar and Navigation, IEE Proceedings, vol. 152, no. 3, pp. 195-205.

[9] T. Lang and G. Hayes, *Exploitation of bistatic Doppler measurements in multistatic tracking*, IEEE Conference on Information Fusion, 2007.

[10] M. Petsios, E. Alivizatos, N. Uzunoglu, *Manoeuvring target tracking using multiple bistatic range and range-rate measurements*, Signal Processing, vol. 87, no. 4, 2007.

[11] B. La Cour, Bayesian *Multistatic Tracking with Doppler-Sensitive Waveforms*, OCEANS 2007, pp. 1-6, June 2007.

[12] K. Kastella and C. Kreucher, *Multiple model Nonlinear Filtering for Low Signal Ground Target Applications*, IEEE Transactions AES, vol. 41, no. 2, pp. 549–564, April 2005.

[13] J. C. Strikwerda, *Finite Difference Schemes and Partial Differential Equations*. New York: Chapman and Hall, 1989.

[14] H. J. Kushner, *Probability Methods for Approximations in Stochastic Control and for elliptic Equations*. Academic Press, 1977.

[15] Y. Bar-Shalom, X. Li, and T. Kirubarajan, *Estimation with Applications to Tracking and Navigation*. New York: John Wiley and Sons, 2001.

[16] C. Kreucher, B. Shapo, and R. Bethel, *Multitarget Detection and Tracking using Multi-sensor Passive Acoustic Data*, IEEE Aerospace Conference, March 2009.

[17] J. C. Toomay and P. J. Hannen Radar Principles, 3rd ed. Norwich, NY: Scitech, 2004.